ACS OMEGA

http://pubs.acs.org/journal/acsodf

Article

One/Two-Step Contribution to Prepare Hierarchical Porous Carbon Derived from Rice Husk for Supercapacitor Electrode Materials

Zhiqin Qin,[§] Yuanyuan Ye,[§] Die Zhang, Jiangling He,* Jiaojiao Zhou, and Jie Cai*

Cite This: *ACS Omega* 2023, 8, 5088−5096

Read Online

ACCESS | Metrics & More | Article Recommendations

ABSTRACT: Grain processing generates vast amounts of agricultural byproducts, and biomass porous carbon electrode materials based on this have attracted broad research interests. Rice husk (RH) is one of the promising feedstocks owing to its good abundance and cheap price. Here, a RH-based porous carbon (RHPC) material was successfully prepared using first-step carbonization and second-step decalcification. The influence of carbonization temperature and decalcification treatment on the structure and electrochemical properties of the RH-based carbon materials were investigated. Thermogravimetric analysis, hydrogen element analysis, scanning electron microscopy, X-ray diffraction, and electrochemical performance tests were used to characterize and analyze the prepared RH-based carbon materials. After carbonization at 1000 °C (RH-1000) and decalcification treatment, RHPC-1000 showed the highest specific surface area of 643.48 m^3/g and the largest pore volume of 0.52 cm^3/g, which were about 1.8 times and 2.5 times that of RH-1000, respectively. RHPC-1000 also possessed a high capacitance retention capability of 97.2% after 10 000 charge−discharge cycles. The results demonstrated the excellent capacitive behavior and superior electrochemical performance of RHPC-1000. In summary, this study reveals a simple and effective preparation method of biomass porous carbon for supercapacitor electrode materials and provides new insight into the high-value utilization of waste biomass resources.

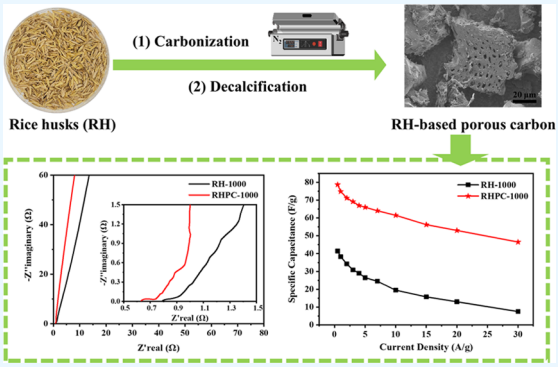

1. INTRODUCTION

With the rapid development of modern society, human beings have become highly dependent on electricity. However, the excessive use of nonrenewable fossil fuels not only faces an energy crisis[1] but also causes environmental pollution and the greenhouse effect.[2] It is urgent to reduce the use of fossil fuels and develop new energy technologies. In recent years, biomass energy has been widely developed, largely because of its clean, renewable, and low-carbon properties.[3] Biomass materials mainly include forest residues, wood waste, poultry waste, agricultural and food byproducts, and so on.[4−6] The carbon materials derived from these biomasses have adjustable physical and chemical activity and can be used as electrodes of electrochemical energy storage equipment in supercapacitors and batteries, reducing the consumption of fossil fuels and contributing to global environmental and climate problems.[7−10]

Rice husk (RH) is not only a typical agricultural byproduct but also a rich, sustainable, and high-quality biomass resource. RH-based carbon materials can be employed for multiple uses, including biological adsorbent for dyes, heavy metal and pesticide residues,[11−13] mortar and concrete additives in building materials,[14−16] biological composite with starch,[17] etc. In particular, RH-based carbon materials showed promising applications in electrochemistry,[18−21] mainly attributed to their composition and properties. RH contains abundant cellulose, hemicellulose, and lignin, and it can be used as an important natural source of multifunctional carbon materials after pyrolysis.[22] About 20% of amorphous silica is distributed in the cell and intercellular layer of RH, and it can be used as a natural template of mesoporous carbon materials with multilayer pore structures for the enhancement of the specific surface area and electrochemical performance of carbon materials.[23] Most studies so far have focused on the reduction, modification, and activation of RH using catalysts and the synthesis of RH-based composite materials.[24−26] Lv et al. synthesized rice husk-based activated carbon through pyrolysis and simultaneous KOH-activation and EDTA-4Na-modification, and the as-prepared carbon materials exhibited high surface areas and rich functional groups as well as good adsorption performance for phenol.[27] Zhang et al. prepared rice husk-based magnetic porous carbon via the pyrolysis of

Received: December 13, 2022
Accepted: January 9, 2023
Published: January 24, 2023

© 2023 The Authors. Published by American Chemical Society

pretreated rice husk with $FeCl_3$ and $ZnCl_2$, and found that as-obtained magnetic porous carbon showed high porosity and magnetization.[28] It is a complicated process and ignores research on the properties and functions of RH. Hence, there is a need for the direct investigation of pure RH-based carbon materials.

In this study, we introduced a simple method for preparing RH-based porous carbon (RHPC) and investigated the impact of carbonization temperature on the structure and electrochemical performance of porous carbon. The structure of the prepared carbon materials was characterized by thermogravimetric analysis, hydrogen elemental analysis, scanning electron microscopy, and X-ray diffraction. The electrochemical performance of the RH-based carbon materials was evaluated by cyclic voltammetry, galvanostatic charge−discharge, and electrochemical impedance spectroscopy measurements. Supercapacitor electrode materials, obtained with a carbonization temperature of 1000 °C and decalcification treatment, showed an abundant microporous structure, a large specific surface area, a uniform pore size, and a superior electrochemical performance. Generally, this research is expected to enrich the application of RH in the electrode material of biomass porous carbon supercapacitors and provide new insight into the high-value utilization of other waste biomass resources.

2. EXPERIMENTAL SECTION

2.1. Materials. Rice husk (RH) was purchased from Alibaba Co., Ltd. (China). Hydrochloric acid (36−38%, HCl), sodium hydroxide (NaOH), and potassium hydroxide (KOH) were provided by Sinopharm Chemical Reagents Co., Ltd. (China). All chemicals were analytical-grade reagents. Deionized water was used throughout the research work (Millipore).

2.2. Preparation of RH-Based Porous Carbon Materials. RH was washed with deionized water and dried in an oven at 100 °C for 10 h. The dried RH was carbonized at different temperatures (400, 600, 800, 900, and 1000 °C) for 2 h under nitrogen (N_2) protection with a temperature rate of 4 °C/min. The as-prepared carbon materials were designated as RH-400, RH-600, RH-800, RH-900, and RH-1000, respectively.

The carbonized samples were soaked with 10% HCl for 3 h to remove Ca, K, and other inorganic salts and then washed with deionized water until the solutions were neutral. The samples were subsequently refluxed with NaOH (2 mol/L) at 80 °C for 2 h to clear SiO_2. The decalcified samples were labeled as RHPC-400, RHPC-600, RHPC-800, RHPC-900, and RHPC-1000, respectively.

2.3. Preparation of Working Electrodes. Nickel foam (1 cm × 2 cm) was sonicated in acetone and deionized water for 10 min and left to dry at room temperature. The RH-based carbon material (0.08 g), carbon black (0.015 g), and poly(vinylidene fluoride) (PVDF, 0.005 g) were successively added into a mortar and ground to homogeneity with a pestle, and then *N*-methyl pyrrolidone (NMP) was added dropwise until a homogeneous slurry was formed. This slurry was pressed uniformly on a foam nickel current collector and dried at 80 °C to obtain the RH-based carbon material working electrode.

2.4. Material Characterization. Thermogravimetric analysis (TGA) was performed to test the thermal stability of RH using a TGA/DSC 1/1100SF instrument (Mettler Toledo, Switzerland). The heating rate was 10 °C/min from room temperature to 1000 °C under a N_2 atmosphere. The hydrogen content of the carbonized RH was determined by a Vario EL Cube elemental analyzer (Elementar, Germany). The morphology of samples was observed using a S-3000N scanning electron microscope (SEM, Hitachi, Japan). The crystal structure of the as-prepared materials was characterized by a X-ray diffractometer (PANalytical Empyrean) equipped with Cu Kα radiation. N_2 adsorption−desorption isotherms were determined at 77.3 K using a JW-BK112 surface area and pore size analyzer, and the specific surface area and pore volume of the samples were calculated with the Brunauer−Emmett−Teller (BET) methods.

2.5. Electrochemical Characterization. Cyclic voltammograms (CV), galvanostatic charge−discharge curves (GCD), and electrochemical impedance spectroscopy (EIS) data were recorded using a CHI 760E electrochemical workstation (Shanghai Chenhua, China). In a typical three-electrode system, the RH-based carbon material was used as the working electrode, a platinum foil Pt plate was used as the counter electrode, and saturated Hg/HgO (6 M KOH) was used as the reference electrode.

2.6. Statistical Analysis. All experiments were performed independently in triplicate, with results presented as mean ± standard deviation (SD).

3. RESULTS AND DISCUSSION

3.1. Thermogravimetric Analysis. The thermogravimetric analysis (TGA) curve of RH following increasing temperatures is illustrated in Figure 1. It was seen that there was a slight weight loss of the RH before 200 °C, which can be

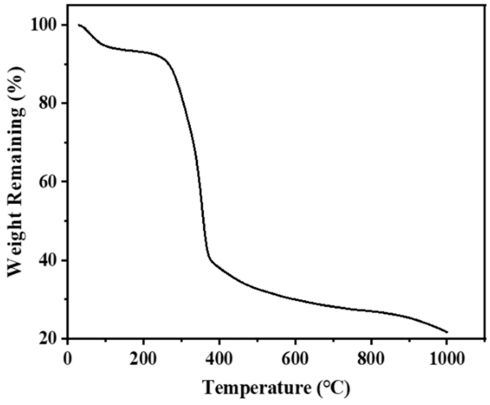

Figure 1. TGA profile of RH.

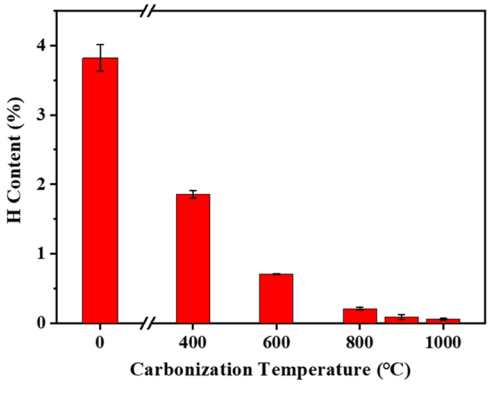

Figure 2. Hydrogen element analysis of RH-based carbon materials.

https://doi.org/10.1021/acsomega.2c07932
ACS Omega 2023, 8, 5088−5096

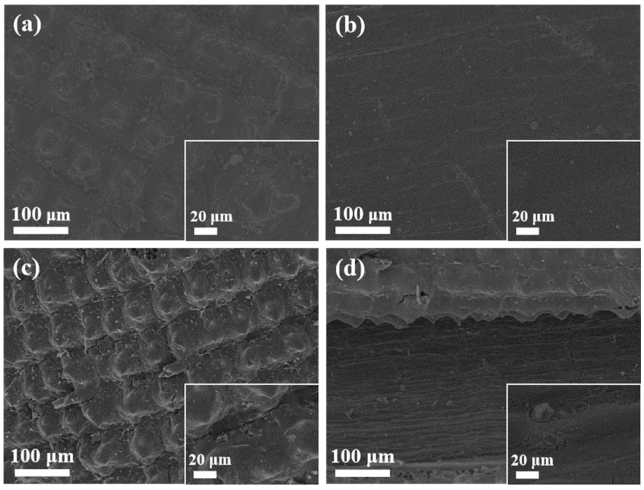

Figure 3. SEM images of (a) the outer surface and (b) inner surface of RH and (c) the outer surface and (d) inner surface of carbonized RH without grinding.

ascribed to the physical effect of water evaporation.[29] RH showed a swift mass loss of ∼53.4% in the temperature range of 200−380 °C, corresponding to the decomposition of natural fats, hemicellulose, and waxy substances, accompanied by the escape of volatile matters.[30] At temperatures higher than 380 °C, a further mass loss of ∼17.2% occurred because of the thermal decomposition of lignin in the RH.[31] A total mass loss of 78% was observed in the studied temperature range after the above three decomposition stages. The residual mass was approximately 22%, consistent with other recent findings.[32]

3.2. Hydrogen Element Analysis. From the hydrogen (H) element analysis of RH-based carbon materials in Figure 2, it was found that the H content in RH-based carbon materials decreased markedly with increasing carbonization temperature (from ∼1.9% at 400 °C to 0.06% at 1000 °C). During carbonization, cellulose and hemicellulose in RH were dehydrated to produce alcohols, ketones, and phenols, and lignin was pyrolyzed to produce oxygenated aliphatic and aromatic components, and the formed gas products such as H_2O, CO_2, CO, and H_2 escaped, thus resulting in the promotion of H reduction.[33,34] It was concluded that cellulose, hemicellulose, and lignin in RH were maximally degraded at 1000 °C.[35]

3.3. Morphology of the RH-Based Carbon Material. The inner and outer surface morphologies of the RH before and after the carbonization process were visualized by scanning electron microscopy (SEM). It is clearly observed that the outer surface of the RH had orderly convex structures (Figure 3a), while the inner surface presented a dense structure with a smooth surface (Figure 3b). After carbonization, the outer surface of the RH-based carbon material (Figure 3c) appeared to have obvious cracks and became very rough, while the inner surface (Figure 3d) showed a layered structure, which was associated with the pyrolysis of organic molecules during the carbonization process.[36] At higher carbonization temperatures, a large number of cellulose and hemicellulose in RH were pyrolyzed into volatile small molecules such as H_2O, H_2, and CO and escaped from the surface, which led to an obvious increase in the surface area. This finding is consistent with the reported work.[37]

The microstructures of the carbonized samples at different temperatures are shown in Figure 4. Little change in the overall macrostructure of the RH-based carbon material was observed, which was related to the RH raw material itself.[38] However, the carbonization temperature had some influence on the micromorphology of the RH-based carbon material. With the temperature increasing, the organic components in the RH were pyrolyzed, and the released low-molecular volatiles facilitated the formation of the pore structure, resulting in a noticeable rough morphology with cracks.[39,40] At a lower carbonization temperature, the RH-based carbon material showed an uneven surface morphology owing to the loss of water and incomplete decomposition of biomass in the RH.[32] When the carbonization temperature was above 900 °C, crystallization occurred in the RH, and the structure became clear and orderly arranged. When the carbonization temperature reached 1000 °C, according to the previous thermogravimetric analysis and hydrogen element analysis, the cellulose, hemicellulose, and lignin in the RH were basically decomposed, and thus the obtained RH-based carbon material showed a highly uniform pore size and a relatively high specific surface area and pore volume.[41]

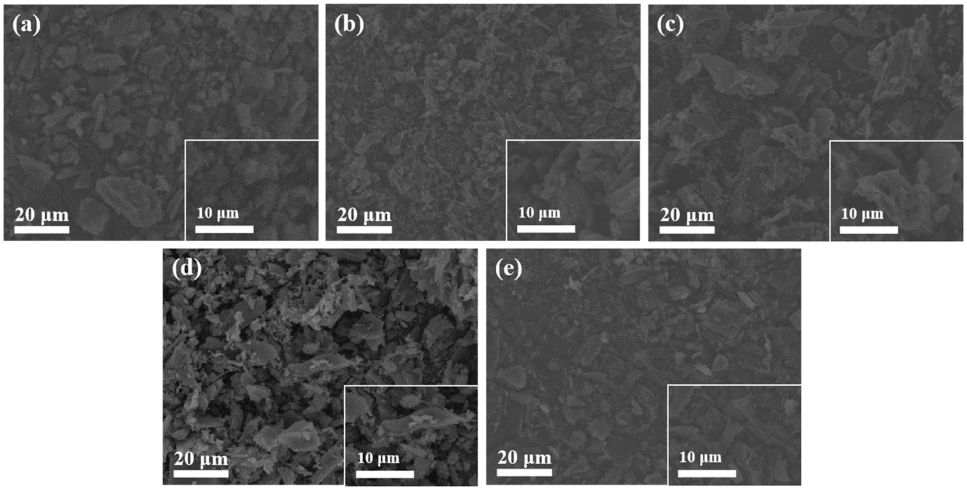

Figure 4. SEM micrographs of the RH-based carbon materials carbonized at different temperatures: (a) 400 °C, (b) 600 °C, (c) 800 °C, (d) 900 °C, and (e) 1000 °C.

https://doi.org/10.1021/acsomega.2c07932
ACS Omega 2023, 8, 5088−5096

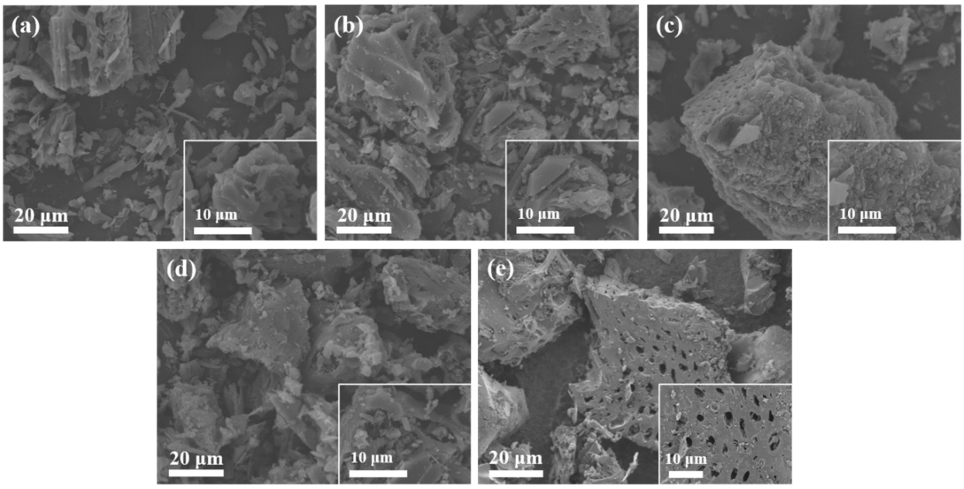

Figure 5. SEM micrographs of the decalcified RH-based carbon materials carbonized at different temperatures: (a) 400 °C, (b) 600 °C, (c) 800 °C, (d) 900 °C, and (e) 1000 °C.

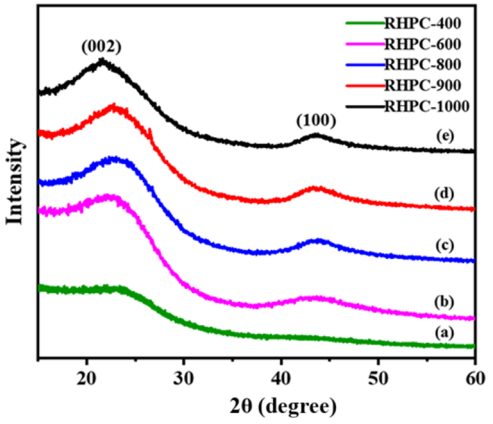

Figure 6. XRD patterns of RHPCs carbonized at different temperatures: (a) 400 °C, (b) 600 °C, (c) 800 °C, (d) 900 °C, and (e) 1000 °C.

Table 1. Specific Surface Areas, Pore Volumes, and Average Adsorption Pore Sizes of RH-Based Carbon Materials

material	specific surface area (m^3/g)	pore volume (cm^3/g)	average adsorption pore size (nm)
RH-400	6.56	0.03	17.77
RH-600	18.57	0.04	8.50
RH-800	30.26	0.05	6.57
RH-900	289.41	0.18	2.35
RH-1000	356.22	0.21	2.28
RHPC-400	10.78	0.04	12.58
RHPC-600	163.63	0.22	5.33
RHPC-800	159.65	0.24	5.95
RHPC-900	530.20	0.45	3.34
RHPC-1000	643.48	0.52	3.21

3.4. Morphology of RHPC. Figure 5 shows the microscopic morphology of the RH-based carbon materials after

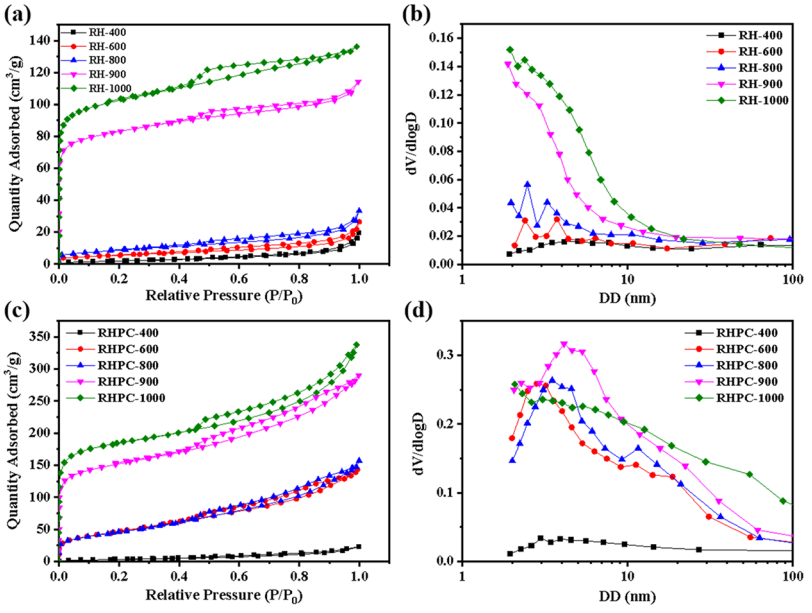

Figure 7. N_2 adsorption−desorption isotherms and the corresponding pore size distribution curves of RH-based carbon materials before (a, b) and after (c, d) decalcification.

https://doi.org/10.1021/acsomega.2c07932
ACS Omega 2023, 8, 5088−5096

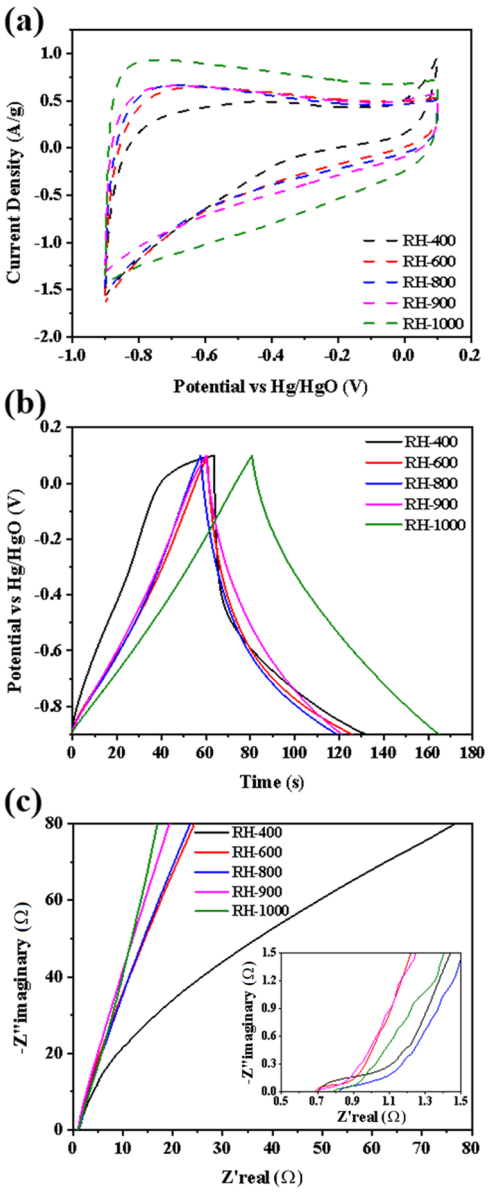

Figure 8. (a) CV curves, (b) galvanostatic charge−discharge (GCD) curves, and (c) EIS patterns of RHs carbonized at different temperatures.

decalcification treatment at different carbonization temperatures. It could be seen that there were obvious differences in the microstructure of the deashing RHPCs after being carbonized at various temperatures, which might be attributed to the different degrees of residual substances after decomposition, such as inorganic salts (like calcium and potassium) and silicon dioxide. It was also shown that RHPC-1000 had the highest porosity and the largest specific surface area among other RHPCs.

3.5. X-ray Diffraction (XRD) Analysis. Figure 6 illustrates the XRD patterns of RHPCs prepared at 400, 600, 800, 900, and 1000 °C. RHPC is composed of crystals and also semicrystals. Two broad peaks at approximately 22.3 and 43.5° are attributed to the typical (002) and (100) reflections of the disordered carbon layer, respectively.[35] The existence of the obvious diffraction peaks on the (002) and (100) crystal planes revealed that there were numerous graphite microcrystalline structures in RHPCs prepared at 600−1000 °C. The (002) reflections between 20 and 30° become gradually narrowing and strong with increasing carbonization temperature, indicating that a high temperature could enhance the electric conductivity of carbon materials.[42] This is related to the increased graphitization degree of carbon materials, as previously reported.[43]

3.6. BET Analysis. The adsorption−desorption isotherm, pore size distribution, and corresponding specific surface area of RH-based carbon materials under different treatment conditions before and after decalcification were measured using the BET method (Figure 7). Figure 7a,b show the adsorption−desorption curves and pore size distributions of the five RH-based carbon materials before decalcification. The isotherms of RH-400, RH-600, and RH-800 showed typical type II curves, while the isotherms of RH-900 and RH-1000 exhibited typical type I curves, which were associated with micropores in samples. For temperatures ≤ 800 °C, the tar compound formed in the carbonization process blocked the pores, resulting in a decrease in the specific surface area. For temperatures ≥ 900 °C, the specific surface area of RH and RHPC increased significantly, mainly owing to the fact that the water molecules under high-temperature conditions can behave as an activator, promoting the reaction in the surface of carbon materials and the formation of micropores.[44] Figure 7c reveals that all of the isotherms of RHPC had typical type II curves, except for the isotherm of RHPC-400 with a type I curve. Figure 7d suggests that appropriate heat treatment temperature contributed to the formation of macropores in RHPC.[45] The results presented in Table 1 demonstrate that RH-1000 and RHPC-1000 had the highest specific surface areas, the largest pore volumes, and appropriate pore size distribution. During the process of decalcification, the removal of tar compounds and the dissolution of some inorganic salts and silica led to the formation of micropores in the carbon material, which significantly increased its specific surface area.[46] Therefore, the specific surface area for RHPC-1000 stands out among other samples.

3.7. Electrochemical Performance of the RH-Based Carbon Material. Figure 8a presents the cyclic voltammetry (CV) curves of the RH-based carbon material under different carbonization temperatures at a scanning rate of 20 mV/s. The CV curves of all samples exhibit a good rectangular shape with typical electric double-layer capacitance, suggesting fast charge and discharge characteristics.[35] It was obvious that RH-1000 had the highest CV area and specific capacitance and exhibited more excellent capacitive behavior compared with other RH-based carbon materials. Figure 8b displays the galvanostatic charge−discharge (GCD) curves of RH samples at a current density of 0.5 A/g. The RH-based carbon materials carbonized at higher temperatures showed higher specific surface areas and pore volumes; thus, the discharge time of RH-1000 was markedly longer than that of other RH-based carbon materials at the same current density. These indicated that RH-1000 provided greater capacitance, consistent with the results of the CV test. The electrochemical impedance spectroscopy (EIS) curve was performed to characterize the ion transfer behavior and resistance of the electrode material (Figure 8c). In the high-frequency region, the intersection of the semicircle and the abscissa and its diameter represent the equivalent series resistance and charge transfer resistance, respectively.[47] The larger the semicircle diameter, the greater the charge transfer resistance. In the low-frequency region, the larger slope indicates the ideal capacitive behavior of the carbon

https://doi.org/10.1021/acsomega.2c07932
ACS Omega 2023, 8, 5088−5096

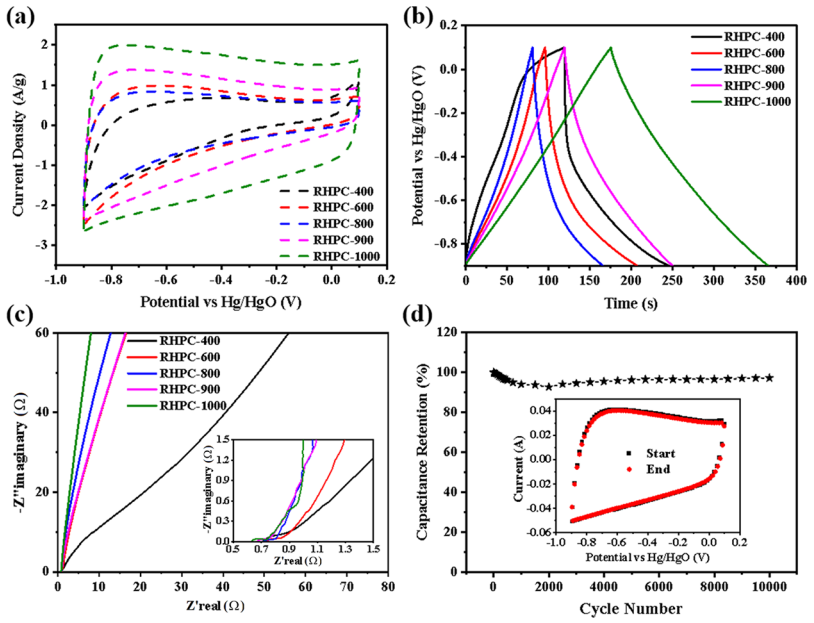

Figure 9. (a) CV curves, (b) GCD curves, and (c) EIS patterns of RHPCs carbonized at different temperatures. (d) Cycling stability of RHPC-1000 for 10 000 charge−discharge cycles.

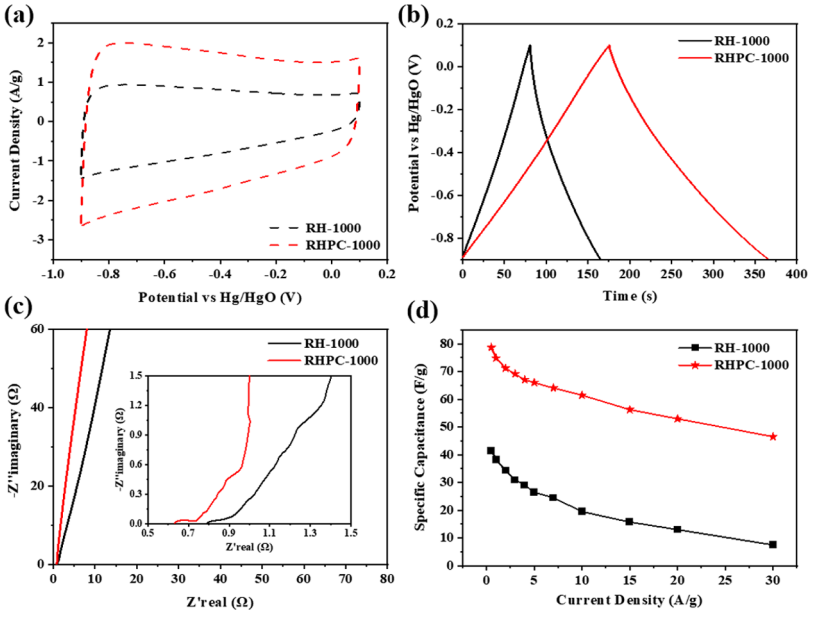

Figure 10. (a) CV curves, (b) GCD curves, and (c) EIS patterns of RH-1000 and RHPC-1000. (d) Comparison of the specific capacitance of RH-1000 and RHPC-1000 at different current densities.

materials.[48] It was found that RH-1000 had the smallest charge transfer resistance among the five carbon materials, revealing the relatively higher conductivity and electron transfer rate.[49]

3.8. Electrochemical Performance of RHPC. Figure 9a,b show the CV and GCD plots of RH-based carbon materials after decalcification under the same test conditions. The results showed that the materials after decalcification retained the nonpseudo-capacitance characteristics. All RHPCs showed rectangle-shaped CV curves, exhibiting a typical electrochemical double-layer capacitance behavior.[50,51] The conductivity of RHPCs increased with increasing carbonization temperature, which was associated with the corresponding specific surface area. RHPC-1000 had the highest specific surface area (643.48 m^3/g), resulting in high immigration of the electrolyte ions into the electrode during charging and discharging and leading to the highest specific capacitance (78.70 F/g) in the GCD test.[43] It was found that RHPC-1000 showed relatively small charge transfer resistance and the lowest equivalent series resistance among porous carbon samples (Figure 9c). Figure 9d shows the cycling stability of RHPC-1000 for 10 000 charge−discharge cycles under 200 mV/s extreme scanning, and the CV plots of the 1st and 10 000th cycles were compared in the middle chart. It could be seen that the CV area of the 10 000th cycle was slightly smaller than that of the 1st cycle. It was demonstrated that the specific capacitance decreased gradually in the first 2000 cycles and then remained stable until the end of 1000 cycles, and it

https://doi.org/10.1021/acsomega.2c07932
ACS Omega 2023, 8, 5088−5096

decreased by 2.8% after 10 000 cycles, indicating the excellent cycling stability of RHPC-1000.

3.9. Electrochemical Performance of RH-1000 and RHPC-1000. As shown in Figure 10a, RHPC-1000 exhibited a much higher specific capacitance compared with RH-1000. The corresponding GCD curves presented an almost symmetrical triangle with slight nonlinearities (Figure 10b), demonstrating the fast transmission of ions in the hierarchically porous structure and good electrochemical reversibility. RHPC-1000 had a much longer charge−discharge time than RH-1000, implying the superior rate capability of RHPC-1000, which could be related to the more abundant microporous structure in RHPC-1000, which provided electrolyte channels to enhance the ion transport properties.[52] RHPC-1000 also showed a much smaller equivalent series resistance and charge transfer resistance, compared with RH-1000, indicating a better conductivity and electron transfer rate (Figure 10c). As demonstrated in Figure 10d, RHPC-1000 exhibited much higher specific capacitance and much better rate capability than RH-1000, confirming the excellent electrochemical performance of RHPC-1000.

4. CONCLUSIONS

In this work, we successfully prepared RH-based porous carbon (RHPC) materials by first-step carbonization and second-step decalcification with the use of rice husk (RH). Carbonization temperature and decalcification treatment were found to have implications for the structure, pore size distribution, and specific surface area of carbon materials. It was shown that increasing carbonization temperature resulted in an increase in the specific surface area and pore volume and the formation of a more uniform pore size in RH-based carbon materials. RH-1000 possessed a specific surface area of 356.22 m^3/g and a pore volume of 0.21 cm^3/g. After decalcification treatment, residual silica, some inorganic salts, and tar compounds in the carbon surface and pores were removed, leading to an increase in the amount of micropores of RHPC. RHPC-1000 showed the highest specific surface area (643.48 m^3/g) and pore volume (0.52 cm^3/g). After 10 000 charge−discharge cycles, it maintained an excellent capacitance retention rate (97.2%). RHPC-1000 also exhibited the best electrochemical performance including small transfer resistance, outstanding specific capacitance, and excellent cycling stability. Overall, this study provides a new strategy for the development of supercapacitor electrode materials and sets a solid foundation for the further practical application of RH-based porous carbon.

AUTHOR INFORMATION

Corresponding Authors

Jiangling He − *National R&D Center for Se-Rich Agricultural Products Processing, Hubei Engineering Research Center for Deep Processing of Green Se-Rich Agricultural Products, School of Modern Industry for Selenium Science and Engineering, Wuhan Polytechnic University, Wuhan 430023, China*; Email: hejiangling@whpu.edu.cn

Jie Cai − *National R&D Center for Se-Rich Agricultural Products Processing, Hubei Engineering Research Center for Deep Processing of Green Se-Rich Agricultural Products, School of Modern Industry for Selenium Science and Engineering, Wuhan Polytechnic University, Wuhan 430023, China; Key Laboratory for Deep Processing of Major Grain and Oil, Ministry of Education, Hubei Key Laboratory for Processing and Transformation of Agricultural Products, Wuhan Polytechnic University, Wuhan 430023, China*; orcid.org/0000-0003-3065-6185; Email: caijievip@whpu.edu.cn

Authors

Zhiqin Qin − *National R&D Center for Se-Rich Agricultural Products Processing, Hubei Engineering Research Center for Deep Processing of Green Se-Rich Agricultural Products, School of Modern Industry for Selenium Science and Engineering, Wuhan Polytechnic University, Wuhan 430023, China; Key Laboratory for Deep Processing of Major Grain and Oil, Ministry of Education, Hubei Key Laboratory for Processing and Transformation of Agricultural Products, Wuhan Polytechnic University, Wuhan 430023, China*

Yuanyuan Ye − *National R&D Center for Se-Rich Agricultural Products Processing, Hubei Engineering Research Center for Deep Processing of Green Se-Rich Agricultural Products, School of Modern Industry for Selenium Science and Engineering, Wuhan Polytechnic University, Wuhan 430023, China; Key Laboratory for Deep Processing of Major Grain and Oil, Ministry of Education, Hubei Key Laboratory for Processing and Transformation of Agricultural Products, Wuhan Polytechnic University, Wuhan 430023, China*

Die Zhang − *Key Laboratory for Deep Processing of Major Grain and Oil, Ministry of Education, Hubei Key Laboratory for Processing and Transformation of Agricultural Products, Wuhan Polytechnic University, Wuhan 430023, China*

Jiaojiao Zhou − *National R&D Center for Se-Rich Agricultural Products Processing, Hubei Engineering Research Center for Deep Processing of Green Se-Rich Agricultural Products, School of Modern Industry for Selenium Science and Engineering, Wuhan Polytechnic University, Wuhan 430023, China*

Complete contact information is available at: https://pubs.acs.org/10.1021/acsomega.2c07932

Author Contributions

[§]Z.Q. and Y.Y. contributed equally to this work.

Funding

This research did not receive any specific grant from funding agencies in the public, commercial, or not-for-profit sectors.

Notes

The authors declare no competing financial interest.

REFERENCES

(1) Mufutau Opeyemi, B. Path to sustainable energy consumption: The possibility of substituting renewable energy for non-renewable energy. *Energy* **2021**, *228*, No. 120519.

(2) Shindell, D.; Smith, C. J. Climate and air-quality benefits of a realistic phase-out of fossil fuels. *Nature* **2019**, *573*, 408−411.

(3) Joselin Herbert, G. M.; Unni Krishnan, A. Quantifying environmental performance of biomass energy. *Renewable Sustainable Energy Rev.* **2016**, *59*, 292−308.

(4) Vitale, I.; Dondo, R. G.; González, M.; Cóccola, M. E. Modelling and optimization of material flows in the wood pellet supply chain. *Appl. Energy* **2022**, *313*, No. 118776.

(5) Santos Dalólio, F.; da Silva, J. N.; Carneiro de Oliveira, A. C.; Ferreira Tinôco, I. d. F.; Christiam Barbosa, R.; Resende, M. d. O.; Teixeira Albino, L. F.; Teixeira Coelho, S. Poultry litter as biomass energy: A review and future perspectives. *Renewable Sustainable Energy Rev.* **2017**, *76*, 941−949.

(6) Dugmore, T. I. J.; Clark, J. H.; Bustamante, J.; Houghton, J. A.; Matharu, A. S. Valorisation of biowastes for the production of green materials using chemical methods. *Top. Curr. Chem. (Z)* **2017**, *375*, 46.
(7) Liedel, C. Sustainable battery materials from biomass. *ChemSusChem* **2020**, *13*, 2110−2141.
(8) Rawat, S.; Mishra, R. K.; Bhaskar, T. Biomass derived functional carbon materials for supercapacitor applications. *Chemosphere* **2022**, *286*, No. 131961.
(9) Wang, J.; Nie, P.; Ding, B.; Dong, S.; Hao, X.; Dou, H.; Zhang, X. Biomass derived carbon for energy storage devices. *J. Mater. Chem. A* **2017**, *5*, 2411−2428.
(10) Wang, Y.; Qu, Q.; Gao, S.; Tang, G.; Liu, K.; He, S.; Huang, C. Biomass derived carbon as binder-free electrode materials for supercapacitors. *Carbon* **2019**, *155*, 706−726.
(11) Chuah, T. G.; Jumasiah, A.; Azni, I.; Katayon, S.; Thomas Choong, S. Y. Rice husk as a potentially low-cost biosorbent for heavy metal and dye removal: an overview. *Desalination* **2005**, *175*, 305−316.
(12) Masoumi, A.; Hemmati, K.; Ghaemy, M. Low-cost nanoparticles sorbent from modified rice husk and a copolymer for efficient removal of Pb(II) and crystal violet from water. *Chemosphere* **2016**, *146*, 253−262.
(13) Zhang, H.; Zhang, R.; Li, W.; Ling, Z.; Shu, W.; Ma, J.; Yan, Y. Agricultural waste-derived biochars from co-hydrothermal gasification of rice husk and chicken manure and their adsorption performance for dimethoate. *J. Hazard. Mater.* **2022**, *429*, No. 128248.
(14) Fernando, S.; Gunasekara, C.; Law, D. W.; Nasvi, M. C. M.; Setunge, S.; Dissanayake, R. Life cycle assessment and cost analysis of fly ash-rice husk ash blended alkali-activated concrete. *J. Environ. Manage.* **2021**, *295*, No. 113140.
(15) Thiedeitz, M.; Ostermaier, B.; Kränkel, T. Rice husk ash as an additive in mortar − Contribution to microstructural, strength and durability performance. *Resour., Conserv. Recycl.* **2022**, *184*, No. 106389.
(16) Sonat, C.; Unluer, C. Development of magnesium-silicate-hydrate (M-S-H) cement with rice husk ash. *J. Cleaner Prod.* **2019**, *211*, 787−803.
(17) Kargarzadeh, H.; Johar, N.; Ahmad, I. Starch biocomposite film reinforced by multiscale rice husk fiber. *Compos. Sci. Technol.* **2017**, *151*, 147−155.
(18) Dawei, L.; Xiaoxiao, Z.; Yu, W.; Peijie, Z.; Li, Z.; Zongbo, Z.; Xin, G.; Yingyun, Q.; Guixia, L.; Yuanyu, T. Adjusting ash content of char to enhance lithium storage performance of rice husk-based SiO_2/C. *J. Alloys Compd.* **2021**, *854*, No. 156986.
(19) Deshagani, S.; Krushnamurty, K.; Deepa, M. High energy density, robust and economical supercapacitor with poly(3,4-ethylenedioxythiophene)-CO_2 activated rice husk derived carbon hybrid electrodes. *Mater. Today Energy* **2018**, *9*, 137−153.
(20) Huang, S.-S.; Tung, M. T.; Huynh, C. D.; Hwang, B.-J.; Bieker, P. M.; Fang, C.-C.; Wu, N.-L. Engineering rice husk into a high-performance electrode material through an ecofriendly process and assessing its application for lithium-ion sulfur batteries. *ACS Sustainable Chem. Eng.* **2019**, *7*, 7851−7861.
(21) Jung, D. S.; Ryou, M. H.; Sung, Y. J.; Park, S. B.; Choi, J. W. Recycling rice husks for high-capacity lithium battery anodes. *Proc. Natl. Acad. Sci. U.S.A.* **2013**, *110*, 12229−12234.
(22) Zhang, W.; Jian, W.; Yin, J.; Zhang, X.; Wang, C.; Lin, X.; Qin, Y.; Lu, K.; Lin, H.; Wang, T.; Qiu, X. A comprehensive green utilization strategy of lignocellulose from rice husk for the fabrication of high-rate electrochemical zinc ion capacitors. *J. Cleaner Prod.* **2021**, *327*, No. 129522.
(23) Liu, Y.; Tan, H.; Tan, Z.; Cheng, X. Rice husk derived capacitive carbon prepared by one-step molten salt carbonization for supercapacitors. *J. Energy Storage* **2022**, *55*, No. 105437.
(24) Chen, Z.; Wang, X.; Li, W.; Yang, X.; Qiu, J.; Wang, Z. A low-temperature dehydration carbon-fixation strategy for lignocellulose-based hierarchical porous carbon for supercapacitors. *ChemSusChem* **2022**, *15*, No. e202101918.
(25) Sridevi, V.; Suriapparao, D. V.; Tukarambai, M.; Terapalli, A.; Ramesh, P.; Sankar Rao, C.; Gautam, R.; Moorthy, J. V.; Suresh Kumar, C. Understanding of synergy in non-isothermal microwave-assisted in-situ catalytic co-pyrolysis of rice husk and polystyrene waste mixtures. *Bioresour. Technol.* **2022**, *360*, No. 127589.
(26) Wong, D. P.; Suriyaprabha, R.; Yuvakumar, R.; Rajendran, V.; Chen, Y.-T.; Hwang, B.-J.; Chen, L.-C.; Chen, K.-H. Binder-free rice husk-based silicon-graphene composite as energy efficient Li-ion battery anodes. *J. Mater. Chem. A* **2013**, *2*, 13437−13441.
(27) Lv, S.; Li, C.; Mi, J.; Meng, H. A functional activated carbon for efficient adsorption of phenol derived from pyrolysis of rice husk, KOH-activation and EDTA-4Na-modification. *Appl. Surf. Sci.* **2020**, *510*, No. 145425.
(28) Zhang, S.; Zhu, S.; Zhang, H.; Liu, X.; Xiong, Y. Synthesis and characterization of rice husk-based magnetic porous carbon by pyrolysis of pretreated rice husk with $FeCl_3$ and $ZnCl_2$. *J. Anal. Appl. Pyrolysis* **2020**, *147*, No. 104806.
(29) Razavi, Z.; Mirghaffari, N.; Rezaei, B. Performance comparison of raw and thermal modified rice husk for decontamination of oil polluted water. *Clean: Soil, Air, Water* **2015**, *43*, 182−190.
(30) Kaur, P.; Kaur, P.; Kaur, K. Adsorptive removal of imazethapyr and imazamox from aqueous solution using modified rice husk. *J. Cleaner Prod.* **2020**, *244*, No. 118699.
(31) Gao, Y.; Zhou, R. Y.; Yao, L.; Yin, W.; Yu, J. X.; Yue, Q.; Xue, Z.; He, H.; Gao, B. Synthesis of rice husk-based ion-imprinted polymer for selective capturing Cu(II) from aqueous solution and re-use of its waste material in Glaser coupling reaction. *J. Hazard. Mater.* **2022**, *424*, No. 127203.
(32) Lazzari, L. K.; Zimmermann, M. V. G.; Perondi, D.; Zampieri, V. B.; Zattera, A. J.; Santana, R. M. C. Production of carbon foams from rice husk. *Mater. Res.* **2019**, *22*, No. e20190427.
(33) Chen, C.; Ji, G.; Mu, L.; Zhang, Y.; Li, A. Comprehensive research on the solid, liquid, and gaseous products of rice husk and rice straw torrefaction. *Sustainable Energy Fuels* **2021**, *5*, 687−697.
(34) Galano, A.; Aburto, J.; Sadhukhan, J.; Torres-García, E. A combined theoretical-experimental investigation on the mechanism of lignin pyrolysis: Role of heating rates and residence times. *J. Anal. Appl. Pyrolysis* **2017**, *128*, 208−216.
(35) Chen, Z.; Wang, X.; Xue, B.; Li, W.; Ding, Z.; Yang, X.; Qiu, J.; Wang, Z. Rice husk-based hierarchical porous carbon for high performance supercapacitors: The structure-performance relationship. *Carbon* **2020**, *161*, 432−444.
(36) Satbaev, B.; Yefremova, S.; Zharmenov, A.; Kablanbekov, A.; Yermishin, S.; Shalabaev, N.; Satbaev, A.; Khen, V. Rice husk research: From environmental pollutant to a promising source of organo-mineral raw materials. *Materials* **2021**, *14*, No. 4119.
(37) Alvarez, J.; Lopez, G.; Amutio, M.; Bilbao, J.; Olazar, M. Physical activation of rice husk pyrolysis char for the production of high surface area activated carbons. *Ind. Eng. Chem. Res.* **2015**, *54*, 7241−7250.
(38) Yang, X.; Wang, L.; Guo, J.; Wang, H.; Masek, O.; Wang, H.; Bolan, N. S.; Alessi, D. S.; Hou, D. Aging features of metal(loid)s in biochar-amended soil: Effects of biochar type and aging method. *Sci. Total Environ.* **2022**, *815*, No. 152922.
(39) Liao, W.; Zhang, X.; Ke, S.; Shao, J.; Yang, H.; Zhang, S.; Chen, H. Effect of different biomass species and pyrolysis temperatures on heavy metal adsorption, stability and economy of biochar. *Ind. Crop. Prod.* **2022**, *186*, No. 115238.
(40) Wazir, A. H.; Wazir, I. U.; Wazir, A. M. Preparation and characterization of rice husk based physical activated carbon. *Energy Sources, Part A* **2020**, 1−11.
(41) Claoston, N.; Samsuri, A. W.; Ahmad Husni, M. H.; Mohd Amran, M. S. Effects of pyrolysis temperature on the physicochemical properties of empty fruit bunch and rice husk biochars. *Waste Manage. Res.* **2014**, *32*, 331−339.
(42) Guo, D.; Xin, R.; Zhang, Z.; Jiang, W.; Hu, G.; Fan, M. N-doped hierarchically micro- and mesoporous carbons with superior performance in supercapacitors. *Electrochim. Acta* **2018**, *291*, 103−113.

https://doi.org/10.1021/acsomega.2c07932
ACS Omega 2023, 8, 5088−5096

(43) Wu, Y.; Li, C.; An, J.; Zhang, D.; Gao, L. Ultrasonic-assisted fungi modification of lignocellulose-derived hierarchical porous carbon for efficient desalination. *Desalination* **2022**, *541*, No. 116035.
(44) Zhang, S.; Yu, Y.; Xie, M.; Du, C.; Chen, J.; Wan, L.; Zhang, Y. Clean production of N, O-doped activated carbon by water vapor carbonization/activation of expired coffee for high-volumetric supercapacitor. *Appl. Surf. Sci.* **2022**, *589*, No. 153011.
(45) Wu, Z.; Meng, Z.; Yao, C.; Deng, Y.; Zhang, G.; Wang, Y. Rice husk derived hierarchical porous carbon with lightweight and efficient microwave absorption. *Mater. Chem. Phys.* **2022**, *275*, No. 125246.
(46) Zhang, W.; Lin, N.; Liu, D.; Xu, J.; Sha, J.; Yin, J.; Tan, X.; Yang, H.; Lu, H.; Lin, H. Direct carbonization of rice husk to prepare porous carbon for supercapacitor applications. *Energy* **2017**, *128*, 618−625.
(47) Hou, J.; Mao, X.; Wang, J.; Liang, C.; Liang, J. Preparation of rice husk-derived porous hard carbon: A self-template method for biomass anode material used for high-performance lithium-ion battery. *Chem. Phys.* **2021**, *551*, No. 111352.
(48) Tang, D.; Luo, Y.; Lei, W.; Xiang, Q.; Ren, W.; Song, W.; Chen, K.; Sun, J. Hierarchical porous carbon materials derived from waste lentinus edodes by a hybrid hydrothermal and molten salt process for supercapacitor applications. *Appl. Surf. Sci.* **2018**, *462*, 862−871.
(49) Luo, Z.; Liu, M.; Tang, D.; Xu, Y.; Ran, H.; He, J.; Chen, K.; Sun, J. High H_2O_2 selectivity and enhanced Fe^{2+} regeneration toward an effective electro-Fenton process based on a self-doped porous biochar cathode. *Appl. Catal., B* **2022**, *315*, No. 121523.
(50) Teo, E. Y. L.; Muniandy, L.; Ng, E.-P.; Adam, F.; Mohamed, A. R.; Jose, R.; Chong, K. F. High surface area activated carbon from rice husk as a high performance supercapacitor electrode. *Electrochim. Acta* **2016**, *192*, 110−119.
(51) Huang, Y.; He, J.; Luan, Y.; Jiang, Y.; Guo, S.; Zhang, X.; Tian, C.; Jiang, B. Promising biomass-derived hierarchical porous carbon material for high performance supercapacitor. *RSC Adv.* **2017**, *7*, 10385−10390.
(52) Chen, J.; Liu, J.; Wu, D.; Bai, X.; Lin, Y.; Wu, T.; Zhang, C.; Chen, D.; Li, H. Improving the supercapacitor performance of activated carbon materials derived from pretreated rice husk. *J. Energy Storage* **2021**, *44*, No. 103432.

https://doi.org/10.1021/acsomega.2c07932
ACS Omega 2023, 8, 5088−5096